Improvement of Cusp Type and Traveling Wave Type Plasma Direct Energy Converters Applicable to Advanced Fusion Reactor

H. Takeno 1), N. Sotani 1), M. Kume 1), Y. Yasaka 1)

1) Department of Electrical and Electronic Engineering, Kobe University, Kobe 657-8501, Japan

E-mail contact of main author: takeno@eedept.kobe-u.ac.jp

Abstract. A development of research on a direct energy conversion system applicable to an advanced fusion reactor is presented. Recovery of degradation of conversion efficiency due to an energy broadening of the particles has been studied for both cusp type and traveling wave type direct energy converters (CUSPDEC and TWDEC). Following to the scheme presented in the previous paper, experimental investigation has been progressed. Concerning the two-stage deceleration scheme in CUSPDEC, in which low energy ions reflected and lost in a simple deceleration scheme are received by a sub-collector, arrival of reflected low energy ions on the sub-collector is significant, and results of basic measurement have been compared with the results of orbit calculation showing a qualitative agreement. By using the same calculation, a real efficiency has been estimated. Using electrodes with some modification of configuration, an efficiency increment by 7–9 % is expected. As for *fan-type TWDEC*, the concept of which is separation of orbits and electrode arrangement according to ion energies, an experimental simulator of the reduced model: *dual-beam TWDEC* has been constructed. The orbits of ions consistent with the design have been confirmed, and a fast switching operation of extracting voltage provides that a 'dual' energy beam has been successfully extracted and guided along the designed routes.

1. Introduction

Recent results of fusion researches are remarkable in plasma parameters, and an outlook of an advanced fusion can be expected. In the advanced fusion, high social acceptability is expected as it reduces radioactivity problem and direct energy conversion is applicable. In this sense, a development of direct energy conversion (DEC) system is significant.

The authors and collaborators are continuing works for a development of DEC system[1, 2, 3], which is illustrated in FIG. 1. The plasma from the reactor is flowing into a cusp type direct energy converter (CUSPDEC), where particles are discriminated into electrons, thermal ions, and high energy fusion-produced ions such as protons of D-^{3}He reaction. DC electric power is obtained in the CUSPDEC by conventional electrostatic converters for the electrons and the thermal ions. The high energy ions are introduced into a traveling

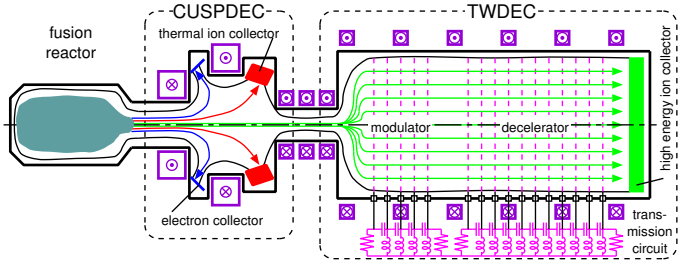

FIG. 1. Diagram of a direct energy conversion system.

wave type direct energy converter (TWDEC), and their energy is recovered by RF electric power. Momota et al. presented a conceptual design of D-^{3}He fusion reactor which consisted of an FRC (Field Reversed Configuration) reactor and two types of direct energy converters[4]. In the design, conversion efficiencies of 65 % of CUSPDEC and 76 % of TWDEC provides 1 GW electricity.

The present main subject for these converters is an improvement of conversion efficiencies for the case of objective particles with a wide energy spread. In the previous paper[5], use of distributed electric fields was proposed. By introducing a lateral sub-collector in a CUSPDEC, increment of conversion efficiency by up to ∼15 % could be expected even for a wide energy spread flux. As for TWDEC, conversion efficiency of ∼8 % was reduced due to thermal energy spread, and some recovery was shown by an employment of a fan-shaped electrode system Although these proposals are expectable, an experimental verification is necessary.

In this paper, experimental works with numerical assistances are shown for improvements of CUSP- and TW- DECs efficiencies. As for CUSPDEC, the motion of reflected ions, which is directly related to the two-stage deceleration scheme, has been examined by combining experiments and numerical orbit calculations. As for TWDEC, an experimental simulator of a reduced model of the *fan-type TWDEC* proposed previously has been constructed, and its initial results are presented.

In the following, issues on CUSPDEC and TWDEC are presented in Sections 2 and 3, respectively. The contents are summarized in Section 4.

2. Two-stage Deceleration in a CUSPDEC Simulator

2.1. Experimental Simulator and Scenario of Two-stage Deceleration

The main functions of the CUSPDEC are discrimination of charged particles and energy conversion from electrons and thermal ions. These will be explained with referring FIG. 2 which shows a schematic illustration of a CUSPDEC experimental simulator.

Magnetic coils A and B form a slanted cusp field between them as their radii are different, and the gradient of the field line can be controlled by the ratio between their currents (I_{A} and I_{B}, respectively). As this is a simulator, a plasma source is settled which locates upstream of the cusp field. Supplying argon gas, a plasma is produced by helicon wave excitation with the magnetic field formed by coils C_1 and C_2. The extraction electrode can be biased to the main chamber (voltage V_{ex}). The particles flowing into the cusp field are detected by four electrodes ($\mathrm{P}_1 \sim \mathrm{P}_4$). $\mathrm{P}_1 \sim \mathrm{P}_3$ are plates and P_4 is a plate with a hole at center, but it can be replaced by a mesh electrode. P_3 and P_4 can be movable in the axial direction with keeping their axial interval constant. The RF for plasma production is modulated by continuous pulses (∼500 Hz and duty ratio of ∼30 %), and a synchronously working boxcar integrator is used in the following measurements.

When V_{ex} is low positive, the produced plasma is flowing into the cusp field. As the electrons are strongly magnetized, their orbits are deflected along the field lines. They go towards the line cusp and are caught by P_1 or P_2. On one hand, magnetization of the

ions is weak, and they almost go straight toward the point cusp. They are flowing into P_3 or P_4. Thus, particle discrimination is achieved.

Energy conversion is achieved when electric loads are connected between electrodes and the earth. The ions toward the point cusp electrodes feel a retarding field as the connected loads generate a positive potential on the electrodes (a negative potential for electrons in the line cusp). The high energy ions overcome the field and can reach the electrodes, but the low energy ions cannot reach, that means fail in energy conversion. As the thermal ions have a wide energy spread, some part of the ions are lost and the conversion efficiency is limited to be low.

The two-stage deceleration scheme was proposed to improve the conversion efficiency. As in FIG. 3, which indicates the dashed rectangular area of FIG. 2, large part of the ions reflected by the retarding field go around P_1. If we use P_1 as an ion collector, the lost energy can be recovered and the conversion efficiency is improved. The destination of electrons can be controlled by the gradient of magnetic field line (I_A/I_B), so we can set only P_2 as an electron collector. This is a scenario of the two-stage deceleration scheme in the present simulator.

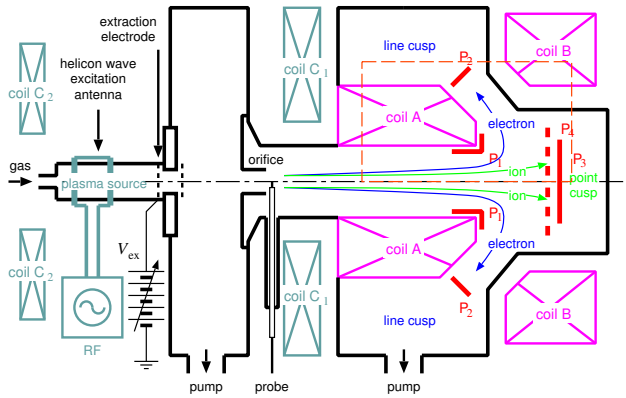

FIG. 2. Schematic illustration of a CUSPDEC experimental simulator.

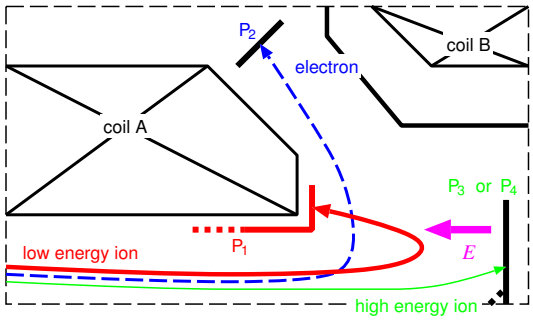

FIG. 3. Orbits of particles in the two-stage deceleration scheme.

2.2. Experimental Results

The extracted ions have been measured by P_3 with negatively biased P_4 of a mesh electrode (voltage of P_4: $V_4 = -200\,\mathrm{V}$). Figure 4 shows voltage(V_3)-current(I_3) characteristics of P_3 for several cases of V_{ex}. In the high V_3 region, electron currents can be seen, which must be due to secondary electrons produced by ion collision to P_4. The region of V_3 detecting the ion current well corresponds to ion energy, that is, $V_3 \leq V_{ex}$.

In order to examine the energy distribution of ions ($f(E)$; E is an ion energy), we have estimated by $I_3(V_3) \propto \int f(E)\sqrt{E - eV_3}\mathrm{d}E$ (e is a unit charge). As for $f(E)$, we have assumed $f(E) \propto \exp(-(E - eV_{ex})^2/E_d^2)$ to express an energy broadening effect by E_d as the plasma source is driven by an RF. In FIG. 5, calculated results for $V_{ex} = 0.8\,\mathrm{kV}$ and $E_d = 20, 40, 60, 80, 100\,\mathrm{eV}$ are shown. In the figure, measured I_3 for $V_{ex} = 0.8\,\mathrm{kV}$ is also shown with compensating constant electron current. According to FIG. 5, the experimental result is similar to the case of $E_d = 60\,\mathrm{eV}$, and this is common for other V_{ex} cases. In the following, we proceed the analysis using this value.

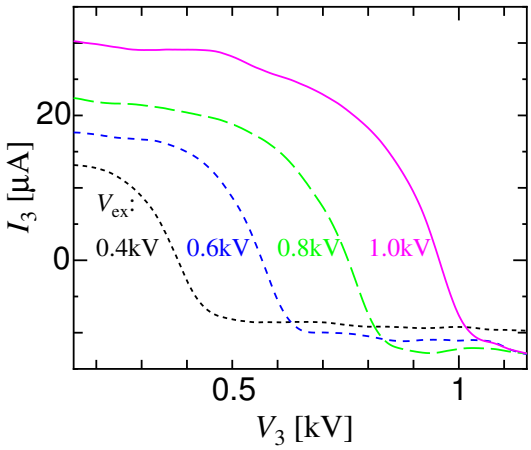

FIG. 4. Voltage-current characteristics of P_3 *electrode for several cases of* V_{ex}.

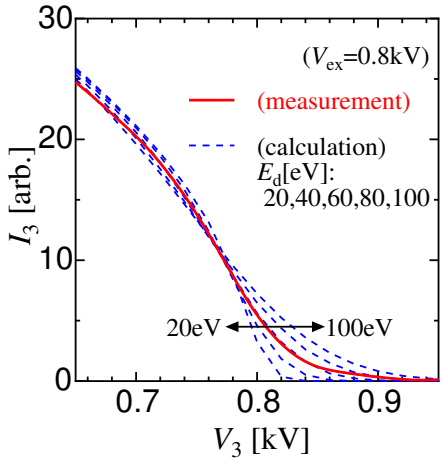

FIG. 5. Comparison of voltage-current characteristics between measured and calculated results.

The detection of reflected ions has been examined in the next. In this measurement, the axial distance between P_4 and P_1 is set to be 73 mm. Figure 6 shows the results of voltage(V_1)-current(I_1) characteristics of P_1. The external conditions are V_{34} (P_3 and P_4 of a mesh electrode are electrically connected in parallel) and V_{ex}, which are varied systematically. The electron currents are also observed for high V_1 region, which may be due to secondary electrons produced on P_3 or P_4. According to the figure, it is seen that larger I_1 is observed as V_{34} becomes larger, and the V_1 regions of the ion current correspond to both V_{34} and V_{ex} ($V_3 \leq V_{limit}$, where V_{limit} is a less value between V_{34} and V_{ex}).

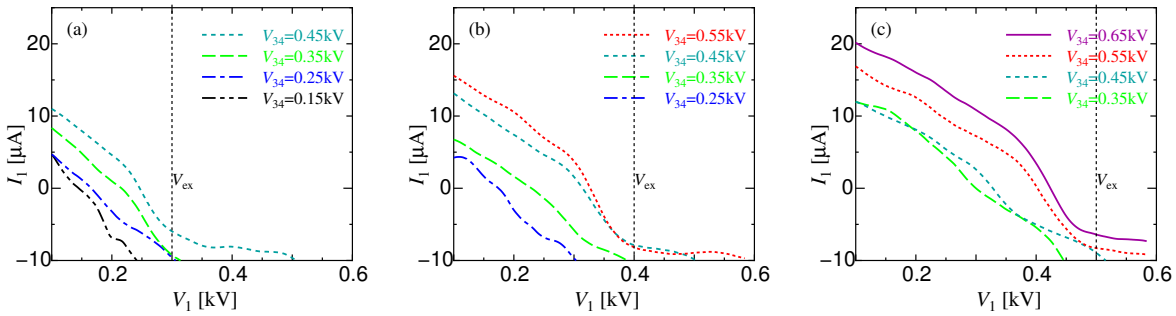

(a) $V_{ex} = 0.3\,\mathrm{kV}$ (b) $V_{ex} = 0.4\,\mathrm{kV}$ (c) $V_{ex} = 0.5\,\mathrm{kV}$

FIG. 6. Measured voltage-current characteristics of P_1 *electrode for several kinds of voltages of* P_{34} *electrodes and several cases of* V_{ex}.

We examine this reflection process by employing orbit calculations. The motion of ions in the CUSPDEC simulator has been solved by a Runge-Kutta scheme. The magnetic field has been calculated by numerical integration of Biot-Savart's law, and the electric field has been solved by a finite difference method. The orbits of incident ions have been traced until it arrives at walls, some electrodes, or the entrance. The orbits have been obtained systematically for the conditions of the incident radial position (r) and the incident energy (E).

The relative amount of ions arriving P_1 to total incident ions, which is proportional to I_1, can be estimated by

$$I_1 \propto \iint p(r,E) f_r(r) f_E(E) 2\pi r dr dE / \iint f_r(r) f_E(E) 2\pi r dr dE \quad (1)$$

where $f_r(r)$ and $f_E(E)$ are radial and energy distributions of the incident ions, respectively. Here, $p(r_a, E_a)$ expresses the arrival of the ion at P_1 with the incident radial position and energy of r_a and E_a, respectively, and it is 1 or 0 when the ion arrives or does not, respectively. In the incident cross section ($r \leq 2\,\mathrm{cm}$), we have assumed a uniform distribution ($f_r(r)$ is constant), and an experimentally found energy distribution ($f_E(E) \propto \exp(-(E - eV_{ex})^2/E_d^2)$). For the same conditions as V_1 and V_{34} in the experiments, we have calculated I_1 and show the results in FIG. 7.

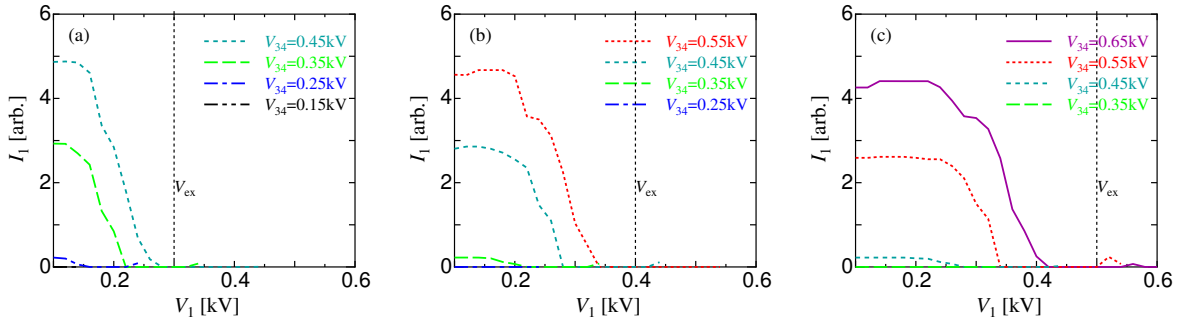

(a) $V_{ex} = 0.3\,\mathrm{kV}$ (b) $V_{ex} = 0.4\,\mathrm{kV}$ (c) $V_{ex} = 0.5\,\mathrm{kV}$

FIG. 7. Calculated voltage-current characteristics of P_1 *electrode for several kinds of voltages of* P_{34} *electrodes and several cases of* V_{ex}.

By comparing between FIG. 6 and FIG. 7, a qualitative agreement is found that larger I_1 is observed as V_{34} becomes larger, and the V_1 regions of the ion current correspond to both V_{34} and V_{ex}. In the quantitative examination, however, some discrepancy are found, such as I_1 on $V_{34} \leq V_{ex}$ of the experiment is relatively larger than those of the calculation.

2.3. Estimation of Real Efficiency

By using the numerical calculation used in the former subsection, we can estimate a real efficiency of two-stage deceleration scheme. We have employed end-loss flux from GAMMA 10 as the objective condition[6], which has $f(E) \propto \sqrt{E - E_s}\exp(-(E - E_s)/T)$ and $E_s = 0.5\,\mathrm{keV}$ and $T = 0.35\,\mathrm{keV}$. In Fig. 11 of Ref. 6, a contour map of expected conversion efficiency (denoted η_{2a} in this paper) for V_1 and V_{34} is presented. This efficiency will be obtained when all of reflected ions arrive at P_1. By using the former orbit calculation, we can obtain an arrival possibility of ions at P_1 (denoted P_a). The real efficiency is obtained by $\eta_2 = \eta_{2inc}P_a + \eta_{1M} = (\eta_{2a} - \eta_{1M})P_a + \eta_{1M}$ where η_{2inc} is the maximum increment of efficiency due to the two-stage deceleration scheme to the optimum efficiency of the one-stage deceleration scheme (η_{1M}).

For the calculation of P_a, we have considered some modification of the electrode configuration. The axial length of P_1 is extended from 5.5 cm to 10 cm, and a cone-shape plate with its height of 1.4 cm is added at the center of P_4. These are indicated by dotted lines in FIG. 3. The results of the calculation is in FIG. 8, where dotted curves indicate η_{2inc} with their values in percent by white letters, and solid curves and color are for P_a with their values in percent by black letters. Around the peak of η_{2inc} ($\sim 0.4\,kV \leq V_1 \leq \sim 0.7\,kV$, $\sim 0.8\,kV \leq V_{34} \leq \sim 1.4\,kV$), the value of P_a is up to $\sim$80 %. The efficiency increment is estimated to be 7–9 %.

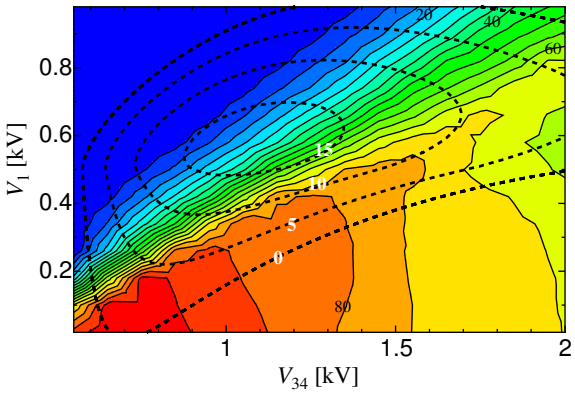

FIG. 8. Two dimensional diagram of improvement of conversion efficiency and arrival possibility of low energy ions for electrodes with modified configuration.

3. Experiments in a Dual-beam TWDEC Device

3.1. Concept of Fan-type TWDEC and Structure of Dual-beam TWDEC

The principle of TWDEC is based on the inverse process of a linear accelerator. An introduced high energy ion flux is velocity-modulated by an RF electric field in a modulator for bunching in the downstream. The bunched beam goes into the decelerator, where traveling RF wave is excited by the bunched beam. An interaction between the beam and the traveling wave resulted that the beam energy is recovered into an RF power in the circuit. The ideal operation is expected when energies of incident particles are monochromatic. However, the ions flowing out from a fusion reactor have a thermal spread, thus the energy conversion efficiency will be reduced. The *fan-type TWDEC* was proposed to recover the efficiency reduction. As shown in FIG. 9, in a fan-type TWDEC, ion orbits are separated by a perpendicular magnetic field. Electrode arrays of modulator and decelerator for each ion should be settled and the corresponding electrodes should be connected. As the ion energy varies continuously, these connected electrodes become a curved surface like a fan.

The experimental simulator *dual-beam TWDEC*, which has the same concept with fan-type TWDEC and a reduced structure, has been constructed (FIG. 10). Two different energy beams are targets, and two electrode arrays are in the optimal positions for each beam energy. The electrically connected corresponding electrodes simulate curved surface electrodes. As in the previous simulator of a usual TWDEC[7], not only the modulator voltage but also the decelerator voltage are supplied externally to examine the deceleration process. At the bottom, Faraday cups (FCPs) are settled for each beam, and their corresponding electrodes are also connected. An electric field is employed as a

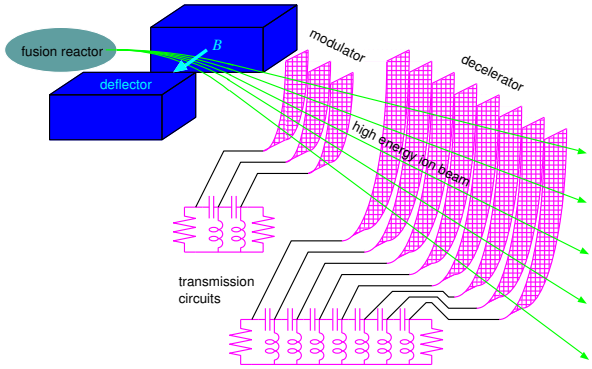

FIG. 9. Conceptual illustration of fan-type TWDEC.

deflector instead of a magnetic field. The ion source is similar to the one in the CUSPDEC simulator, but the extraction voltage V_{ex} can be switched by relatively high frequency. By synchronizing the switching with the pulse of plasma production RF, we can obtain an ion beam with two different energies.

3.2. Experimental Results

The basic structure has been confirmed at first. By setting an appropriate deflection voltage V_D, the extraction voltage V_{ex} has been varied to detect a FCP signal. Figure 11 shows V_{ex} observing a FCP signal versus V_D. The measured data are aligned on two lines irrespective of ion species. In the design, orbits of ions are estimated with an ideal deflection field structure, in which the deflection field only exists between the electrodes. In that calculation, V_{ex} is proportional to V_D and irrespective of ion mass. The relation is indicated by solid and dotted lines in FIG. 11, showing a good agreement with the experimental results.

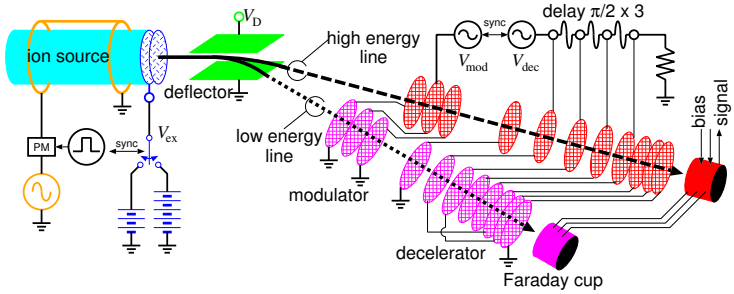

FIG. 10. Schematic illustration of dual-beam TWDEC.

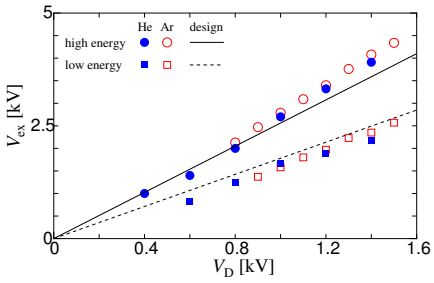

FIG. 11. Extraction voltages observing a Faraday cup signal versus deflection voltages.

Using the results in FIG. 11, a switched operation of V_{ex} has been performed. Figure 12 shows ion distribution functions measured by the FCP. Here, (a) and (b) are for non-switched operations, and (c) is for a switched operation. In the switched operation, the system succeeds in extraction of *dual energy beams*.

We further examine the modulation effect. In the modulation process, ions are velocity modulated, thus their energy broadening is enhanced according to the modulator voltage. We examine variation of full width at half maximum of the beam (ΔE) to the modulator voltage V_{mod}, and the results are summarize in FIG. 13. According to FIG. 13, ΔE slightly increases with an increment of V_{mod}. In a simple consideration, however, the amount of increase of ΔE is expected to be $\sim 2eV_{mod}$. One of the reason of the discrepancy between the results and the expectation may be the structure of the electrodes. The electrodes have a hole, thus the fields between the electrodes are weakened compared with a simple value of the voltage difference over the electrodes distance[7].

4. Summary

Following to the scheme presented in the previous paper, experimental investigations on recovery of the degraded conversion efficiency of DEC devices have been progressed. As for the two-stage deceleration scheme in CUSPDEC, basic measurements on the arrival of reflected low energy ions on the sub-collector have been performed and a reasonable

agreement with the orbit calculation has been obtained. The calculation also enables an estimation of the real efficiency, resulted in an efficiency increment of 7–9 %. The Dual-beam TWDEC simulator of a reduced model of the fan-type TWDEC has been constructed. The fast switching operation of extracting voltage provides that a dual energy beam has been successfully extracted and guided along the designed routes.

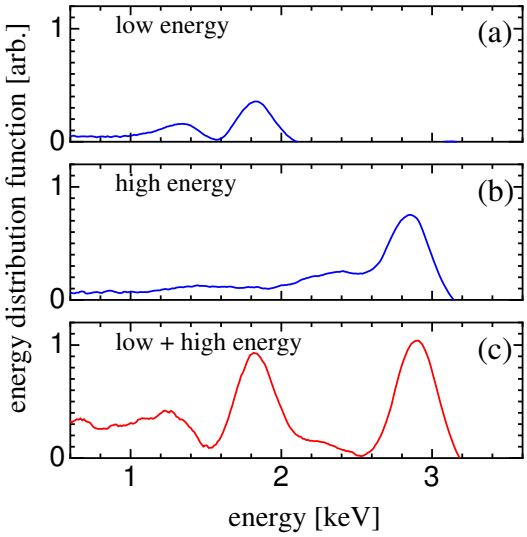

FIG. 12. Examples of measured ion distribution functions.

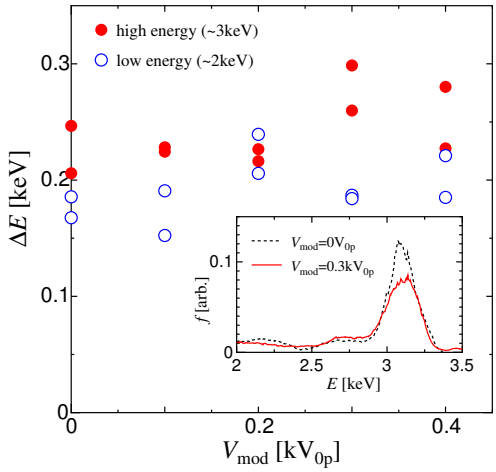

FIG. 13. Measured energy broadenings versus modulator voltages. Inset is samples of energy distribution functions.

Acknowledgments

The authors acknowledge valuable discussions with Drs. Y. Tomita, M. Ishikawa, Y. Nakashima, and I. Katanuma, and experimental assistances by Y. Munakata, H. Ohno, and S. Harada. This work was supported in part by the bilateral coordinated research between Plasma Research Center, University of Tsukuba, National Institute for Fusion Science, and Kobe University. This work was also supported in part by a Grant-in-Aid for Scientific Research (C) (22560273) from Japan Society for the Promotion of Science.

References

[1] Takeno, H., et al., Trans. Fusion Technol., Vol.39, No.1T (2001) pp.386–389.

[2] Tomita, Y., et al., Trans. Fusion Sci. and Technol., Vol.47, No.1T (2005) pp.43–48.

[3] Yasaka, Y., et al., Proc. 22nd IAEA Fusion Energy Conf. (Geneva, Switzerland, 2008) cn165, IC/P4-11.

[4] Momota, H., et al., Proc. 7th Intl. Conf. on Emerging Nuclear Energy Systems (Makuhari, Japan, September 1993) (Singapore: World Scientific, 1993) p 16.

[5] Yasaka, Y., et al., Nuclear Fusion, Vol.49, 075009 (2009) pp.1–9.

[6] Yasaka, Y., et al., Trans. Fusion Sci. and Technol., Vol.55, No.2T (2009) pp.1–8.

[7] Takeno, H., et al., Fusion Eng. Des., Vol.83 (2008) pp.1696–1699.